Journal of Materials Chemistry A

ROYAL SOCIETY OF CHEMISTRY

PAPER

View Article Online
View Journal | View Issue

Cite this: J. Mater. Chem. A, 2023, 11, 4808

Development of rigidity-controlled terpolymer donors for high-performance and mechanically robust organic solar cells†

Jinseck Kim,‡[a] Geon-U Kim,‡[a] Dong Jun Kim,‡[b] Seungjin Lee,[a] Dahyun Jeong,[a] Soodeok Seo,[a] Seo-Jin Ko,*[c] Sung Cheol Yoon,*[c] Taek-Soo Kim*[b] and Bumjoon J. Kim*[a]

Received 24th December 2022
Accepted 9th February 2023

DOI: 10.1039/d2ta09990j

rsc.li/materials-a

Organic solar cells (OSCs) are potential power sources for wearable electronic devices. However, the mechanical stretchability of active materials is not yet sufficient; one of the main reasons is the high rigidity of polymer donors (P_Ds) and the resultant excessive crystalline structures, which makes the active layer mechanically-fragile. In this study, we develop a series of PM6-based terpolymers (PM6-B*X*; *X* = 10–30, *X* indicates the mole percentage of the third component) in which a bulky electro-active third component, 7,8-bis(5-hexylthiophen-2-yl)-11*H*-benzo[4,5] imidazo[2,1-*a*]isoindol-11-one (BID), is introduced to reduce the tightness of their molecular packing. As a result, the neat P_D film with 10 mol% BID (PM6-B10) exhibits significantly improved mechanical ductility (*i.e.*, average crack onset strain (COS_{avg}) of 23.8%) compared to that of the neat PM6 film (COS_{avg} = 14.9%) without a BID unit. In addition, in terms of a blend film, the well-intermixed domains of PM6-B10 and a small molecule acceptor afford OSCs with a high power conversion efficiency (PCE) of 17.2% and mechanical stretchability (COS_{avg} = 11.4%), outperforming the PM6 counterpart (PCE = 15.8%, COS_{avg} = 2.0%). This study suggests important guidelines for the design of efficient P_Ds for high-performance, stretchable OSCs.

1. Introduction

Stretchable organic solar cells (OSCs) are considered potential power sources for next-generation, form factor–free, wearable devices because of their unique features, including light weight and intrinsic mechanical flexibility/stretchability.[1–5] However, the two most important requirements for the stretchable OSCs, high photovoltaic performance and mechanical robustness, are difficult to achieve at the same time, because these two properties typically present a trade-off relationship.[5–8] Especially, state-of-the-art polymer donors (P_Ds) have highly crystalline features with planar and rigid molecular conformation (*e.g.*, PM6 with 4,8-bis(5-(2-ethylhexyl)-4-fluorothiophen-2-yl)benzo[1,2-*b*:4,5-*b*′]dithiophene (FBDT) and 1,3-bis(2-ethylhexyl)-5,7-di(thiophen-2-yl)-4*H*,8*H*-benzo[1,2-*c*:4,5-*c*′]dithiophene-4,8-dione (DTBDD) units) to facilitate π–π intermolecular assembly and enhance electrical properties, however, their mechanical properties in films including tensile properties are poor.[9–12]

In order to enhance the mechanical properties of P_Ds, the high molecular rigidity of polymer chains should be reduced by increasing the chain flexibility.[12–17] A promising strategy to achieve this end is the introduction of flexible spacers through terpolymerization.[12,18–20] For example, Thompson *et al.* reported that a terpolymer (10% T-10-T) with decyl spacers demonstrates an 8-fold increased crack onset strain (COS) than a corresponding polymer without decyl spacers.[19] However, the presence of such electro-inactive spacers in P_Ds often impairs their electrical properties (*i.e.*, charge mobility) due to inhibited intramolecular charge transfer.[21,22] Therefore, it is necessary to explore electro-active (*i.e.*, conjugated) spacers to tune the rigidity of polymer chains without compromising their electrical properties.

Accordingly, an effective molecular design strategy for P_Ds for stretchable OSCs involves the incorporation of bulky electro-active units into the polymer chains, thereby inducing sufficient steric hindrance to reduce the backbone rigidity and enhance the mechanical properties of the P_Ds.[21,22] For example, Bao *et al.* developed a diketopyrrolopyrrole (DPP)-based terpolymer by incorporating a third component that contains a bulky naphthalene side chain, so that relative degree of crystallinity of the polymer significantly decreased from 1 to 0.37.[22] As a result, the

[a]Department of Chemical and Biomolecular Engineering, Korea Advanced Institute of Science and Technology (KAIST), Daejeon 34141, Republic of Korea. E-mail: bumjoonkim@kaist.ac.kr

[b]Department of Mechanical Engineering, Korea Advanced Institute of Science and Technology (KAIST), Daejeon 34141, Republic of Korea. E-mail: tskim1@kaist.ac.kr

[c]Division of Advanced Materials, Korea Research Institute of Chemical Technology (KRICT), Daejeon, 34114, Republic of Korea. E-mail: yoonsch@krict.re.kr; sjko927@krict.re.kr

† Electronic supplementary information (ESI) available. See DOI: https://doi.org/10.1039/d2ta09990j

‡ J. K., G.-U K. and D. J. K. equally contributed to this work.

COS (~15%) of the terpolymer considerably exceeded that (~3%) of the corresponding polymer without the bulky third component. However, although the aforementioned molecular design strategy has been used to enhance the mechanical properties of films based on neat polymers, to the best of our knowledge, this strategy has not yet been explored to enhance the mechanical properties of films based on blends; especially, bulk-heterojunction (BHJ) blends of P_Ds and small molecule acceptors (S_As). While the mechanical properties of blend films are affected by the mechanical properties of each component (*i.e.*, P_D and S_A), the morphological properties, which depend on the thermodynamic miscibility between P_D and S_A, also play an important role to determine both the electrical and mechanical properties of the blends.[11,23–31] Thus, for achieving highly efficient and mechanically robust OSCs, it is important to design terpolymer donors containing appropriate bulky electro-active third components by considering their impact on the mechanical properties of the polymers as well as their blend morphology with S_As.

Herein, we report the development of a series of terpolymers (PM6-B*X*, $X = 10$–30) incorporating electro-active 7,8-bis(5-hexylthiophen-2-yl)-11*H*-benzo[4,5]imidazo[2,1-*a*]isoindol-11-one (BID) units for alleviating the excessive backbone rigidity of PM6. The neat PM6-B10 film shows a significantly higher average COS (COS_{avg}) value of 23.8% than that of the neat PM6 film (14.9%), while showing a comparable hole mobility (μ_h) to that of PM6. Moreover, the PM6-B10:Y6-BO blend film contains a larger fraction of the intermixed domains than the PM6:Y6-BO blend film, leading to superior charge generation and mechanical properties. As a result, the PM6-B10:Y6-BO OSC achieves a high power conversion efficiency (PCE) of 17.2%, outperforming a PM6:Y6-BO OSC (PCE = 15.8%). In addition, the mechanical properties of the PM6-B10:Y6-BO blend film ($COS_{avg} = 11.4\%$ and toughness = 4.1 MJ m^{-3}) are superior to those of the PM6:Y6-BO blend film ($COS_{avg} = 2.0\%$ and toughness = 0.3 MJ m^{-3}). We carefully investigate the impact of the electro-active BID addition on the structural, optical, electrical, and mechanical properties of the PM6-B*X* terpolymers and study the polymer structure–property–device performance relationship in OSCs.

2. Results and discussion

2.1. Material design and terpolymer properties

The molecular structures of the P_Ds featured in this study are described in Fig. 1a. PM6 was selected as a reference P_D owing to its wide light absorption range, high absorption coefficient, and superior charge mobility, which enable the construction of highly efficient OSCs.[32,33] However, the rigid, planar molecular conformation of PM6 (which consists of highly fused FBDT and DTBDD units) and its consequent strong/tight intermolecular assembly lead to poor stretchability in film.[11,34] To reduce the high molecular rigidity of PM6, we employed a terpolymerization strategy, *i.e.*, we incorporated a third component to tune the conformation of the polymer main chain and thus prevent its excessively tight packing.[35,36] Here, to avoid any compromise of the electrical properties, we designed a new electro-active third component (BID unit) for constructing terpolymers. In general, bulky units have been shown to effectively adjust the torsion angle of polymers and induce higher steric hindrance than less bulky units. This steric hindrance manipulates the intermolecular packing of polymers, thereby enhancing the mechanical properties in film.[22,37] In addition, the designed electro-active BID unit preserves good electrical and optical properties better than other reported flexible spacers.[18,20,21,38–41] A series of terpolymers with different BID contents (10 – 30 mol%) was synthesized in this study to simultaneously optimize the electrical and mechanical properties of the terpolymers.

The synthetic scheme and characterization data of the BID monomer (BID-Br) and P_Ds are provided in the ESI (Fig. S1–S4 and Table S1†). The BID monomer was synthesized *via* a condensation reaction between dibromophthalic anhydride and alkyl thiophene substituted *o*-phenylenediamine (Fig. S1†). The P_Ds were polymerized *via* a Stille-coupling reaction and purified by sequential Soxhlet extraction. The molecular structures of the P_Ds were verified by nuclear magnetic resonance (NMR) spectroscopy (Fig. S2†). The presence of the BID units in the terpolymers is confirmed by the characteristic peaks with a chemical shift of 2.7–2.8 ppm in the obtained NMR spectra, which correspond to the protons attached to the α-carbons of the thiophenes in BID. Although these peaks partially overlap with those corresponding to protons attached to the α-carbons of the side-chain thiophenes in FBDT, the increase in intensity of these characteristic peaks in the NMR spectra is consistent with the increasing BID contents of the terpolymers. The number-average molecular weights (M_ns) of the P_Ds, estimated by gel permeation chromatography (GPC), are similar (127–144 kg mol^{-1}); thus, the effect of molecular weight on the optoelectronic/physical properties of the P_Ds can be disregarded (Fig. S3† and Table 1). In addition, PM6 and the terpolymers are acceptably processable in chlorinated solvents, which are generally used to fabricate OSCs (Fig. S4 and Table S1†). The solubility test procedures are detailed in the ESI.†[41]

Density functional theory (DFT) calculations, at the B3LYP/6-31G(*d*,*p*) level, were performed to investigate the structural conformations of the P_Ds (Fig. 1b and S5†). To simplify the DFT calculations, the length of each polymer backbone was shortened to the dimer level and the alkyl chains were represented by methyl groups. According to the calculations, the incorporation of BID in the PM6 backbone effectively modifies its molecular conformation; the largest torsional (or dihedral) angle of PM6 is ~16° whereas that of the PM6-based terpolymers is ~42°. Steric effects between the bulky BID units and the adjacent FBDT units in the terpolymers reduce their planarity. Consequently, excessively tight packing of PM6 is expected to be alleviated as the content of the BID unit increases in terpolymers. The suitable torsion and following mitigated polymer packing tend to afford films with enhanced ductility.[22]

The optical characteristics of the P_Ds were investigated (Fig. 1c, S6,† and Table 1). With increasing BID content, the UV-Vis absorption spectra of the P_D films were blue-shifted and the ratios of the 0–0 transition peak intensity (located at ~615 nm) to the 0–1 transition peak intensity (located at ~575 nm)

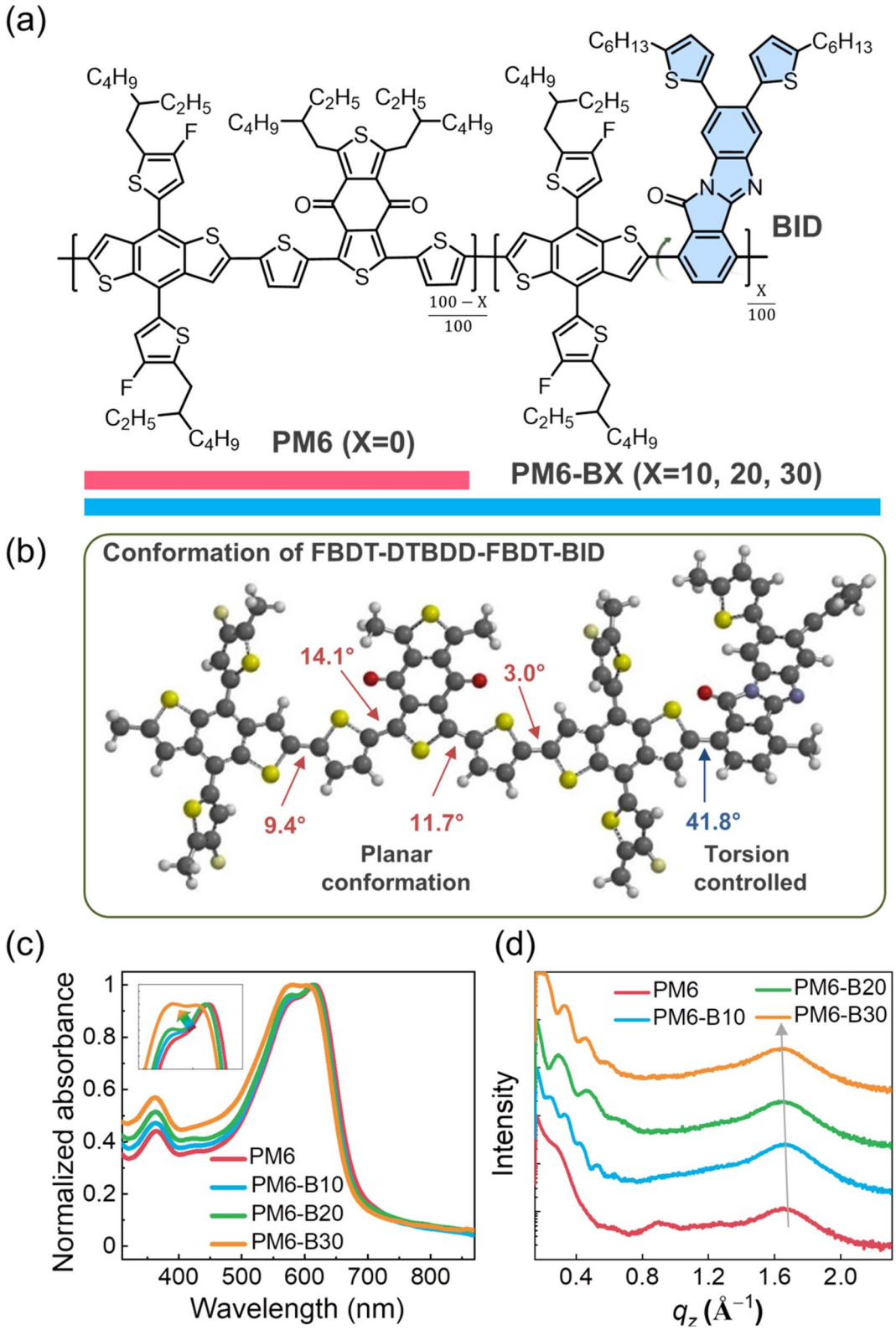

Fig. 1 (a) Molecular structures of P_Ds featured in this study. (b) Simulated molecular conformation of FBDT-DTBDD-FBDT-BID. (c) Normalized UV-Vis absorption spectra (in film) and (d) GIXS line-cut profiles of neat P_D films in the OOP direction.

decreased (Fig. 1c).[42] These results indicate that the molecular packing of the terpolymers was less tight than that of PM6, as expected based on the DFT calculations (Fig. 1b and S5†). To further examine the effect of the BID content on the aggregation behaviors of the P_Ds, we obtained their temperature-dependent UV-Vis absorption in solution (Fig. S6†). The pre-aggregation

Table 1 Material characteristics of P_Ds

P_Ds	M_n ($Đ$)[a] [kg mol^{-1}]	λ_{film}^{max} [b] [nm]	E_g^{opt} [b] [eV]	E_{HOMO} [c] [eV]	E_{LUMO} [d] [eV]	μ_h^{SCLC} ($\times 10^{-4}$) [cm^2 V^{-1} s^{-1}]
PM6	144 (3.66)	615	1.83	−5.53	−3.70	3.5 ± 0.6
PM6-B10	137 (3.21)	614	1.83	−5.55	−3.72	3.2 ± 0.4
PM6-B20	133 (3.20)	613	1.83	−5.56	−3.73	2.3 ± 0.7
PM6-B30	127 (2.96)	578	1.84	−5.56	−3.72	1.6 ± 0.7

[a] Estimated by GPC using 1,2,4-trichlorobenzene as eluent. [b] Determined from UV-Vis absorption spectra of the P_Ds in film. [c] Determined by cyclic voltammetry. [d] Calculated using the equation $E_{LUMO} = E_{HOMO} + E_g^{opt}$.

behaviors of P_Ds play an important role in determining the thin-film morphology and performance of the resulting OSCs.[43,44] In the case of PM6, the 0–0 transition peak remained more prominent compared to the 0–1 transition peak across the entire temperature range, indicating strong pre-aggregation behaviors.[43] Interestingly, the temperature-dependent pre-aggregation (TDA) behaviors of PM6-B10 and PM6-B20 were similar to that of PM6. These terpolymers may preserve short-range ordered aggregation in solution, which can facilitate charge carrier transport in thin film.[43,45] In contrast, in the case of PM6-B30 with its relatively high BID content, the intensity of the 0–0 transition peaks in the UV-Vis absorption spectra gradually decreased with increasing solution temperature, suggesting relatively weak pre-aggregation behaviors.

The electrochemical properties of the P_Ds were investigated by cyclic voltammetry (CV) (Fig. S7†). The highest occupied molecular orbital (HOMO) energy levels of the terpolymers were slightly lower than that of PM6; *i.e.*, the HOMO energy levels of PM6, PM6-B10, PM6-B20, and PM6-B30 were −5.53, −5.55, −5.56, and −5.56 eV, respectively. The substitution of the DTBDD units in PM6 with BID units reduces the number of electron-donating thiophenes, which may partly account for the lower HOMO energy levels of the terpolymers.[46]

The crystalline properties of the P_Ds in film were investigated by grazing incidence wide-angle X-ray scattering (GIXS) (Fig. 1d, S8, and Table S2†). The obtained GIXS linecut profiles in the in-plane (IP) and out-of-plane (OOP) directions are shown in Fig. 1d and S8,† respectively. Distinct (100) and (010) peaks in the GIXS linecut profiles in the IP and OOP directions, respectively, suggest that all the P_Ds have dominant face-on molecular packing orientation, which facilitates vertical charge transport.[47,48] Meanwhile, the crystallinity of the P_Ds decreased with increasing BID content owing to an increase in the torsion of the polymer backbone, which is consistent with the DFT calculations and the results of UV-Vis absorption spectroscopy. For example, the coherence length ($L_{c(010)}$), estimated using the Scherrer equation, of the P_Ds decreased from 27.4 Å for PM6 to 24.8 Å for PM6-B30 (Table S2†).[49] In addition, the π–π stacking distance ($d_{(010)}$) of the P_Ds slightly increased from 3.82 Å for PM6 to 3.85 Å for PM6-B30 (Fig. 1d and Table S2†). To determine the correlation between the crystalline and electrical properties of the P_Ds, their μ_hs were measured using the space-charge limited current (SCLC) method (Table 1).[50] The μ_h of PM6-B10 (3.2×10^{-4} cm^2 V^{-1} s^{-1}) was comparable to that of PM6 (3.5×10^{-4} cm^2 V^{-1} s^{-1}); however, that of PM6-B30 (1.6×10^{-4} cm^2 V^{-1} s^{-1}) was lower.

2.2. Photovoltaic and electrical properties

The photovoltaic performance of the P_Ds developed in this study was evaluated in normal-type OSCs with a configuration of indium tin oxide (ITO)/poly(3,4-ethylenedioxythiophene):poly(styrenesulfonate) (PEDOT:PSS)/active layer/2,9-bis(3-((3-(dimethylamino)propyl)amino)propyl)anthra[2,1,9-*def*:6,5,10-*d*′*e*′*f*′]diisoquinoline-1,3,8,10-(2*H*,9*H*)-tetraone (PDINN)/Ag.[51] The S_A, 2,2′-((2*Z*,2′*Z*)-((12,13-bis(2-butyloctyl)-3,9-diundecyl-12,13-dihydro-[1,2,5]thiadiazolo[3,4-*e*]thieno[2′,3′:4′,5′]thieno[2′,3′:4,5]pyrrolo[3,2-*g*]thieno[2′,3′:4,5]thieno[3,2-*b*]indole-2,10-diyl)bis(methanylylidene))bis(5,6-difluoro-3-oxo-2,3-dihydro-1*H*-indene-2,1-diylidene))dimalononitrile (Y6-BO) was paired with the P_Ds in OSCs owing to its complementary light-absorption properties and appropriately aligned frontier orbital energy levels (Fig. S9†).[52] The current density–voltage (*J*–*V*) curve, PCE distribution, and external quantum efficiency (EQE) spectrum of each OSC are displayed in Fig. 2a–c. The procedures for OSC fabrication and characterization are described in the ESI.† The photovoltaic parameters (open-circuit voltage (V_{oc}), short-circuit current density (J_{sc}), fill factor (FF), and PCE) of the OSCs are listed in Table 2. Interestingly, the PCEs of PM6-B10:Y6-BO (V_{oc} = 0.84 V, J_{sc} = 26.60 mA cm^{-2}, FF = 0.77, and PCE = 17.23%) and PM6-B20:Y6-BO (V_{oc} = 0.85 V, J_{sc} = 26.72 mA cm^{-2}, FF = 0.71, and PCE = 16.06%) OSCs exceeded that of the PM6:Y6-BO OSC (V_{oc} = 0.84 V, J_{sc} = 25.85 mA cm^{-2}, FF = 0.73, and PCE = 15.83%; Table 2). In contrast, the PCE of PM6-B30:Y6-BO OSC (V_{oc} = 0.86 V, J_{sc} = 25.42 mA cm^{-2}, and FF = 0.63, PCE = 13.80%) was lower than that of the PM6:Y6-BO OSC. These results indicate that the incorporation of an optimal amount of BID in PM6 can afford OSCs with enhanced J_{sc}, FF, and PCE. And, the PM6-B10:Y6-BO and PM6-B20:Y6-BO OSCs showed enhanced EQE values in the absorption ranges of P_D and S_A (*e.g.*, 300–400 and 500–800 nm) than those of the PM6:Y6-BO OSC (Fig. 2c). The J_{sc} calculated from the EQE spectrum of each OSC agreed well with its measured J_{sc} (within an error of 4%).

To demonstrate the advantage of employing the highly fused BID unit as the third component in our terpolymerization strategy, another P_D (PM6-P10) was synthesized in which a less fused, more widely used phthalimide unit was incorporated as the third component into PM6. The mole percentage of the phthalimide unit in PM6-P10 was the same as that of BID in PM6-B10 (10 mol%), which exhibited the highest PCE among the BID-based terpolymers (Fig. S10†).[8,53–55] For fair comparison, a batch with a molecular weight (M_n = 131 kg mol^{-1}) similar to

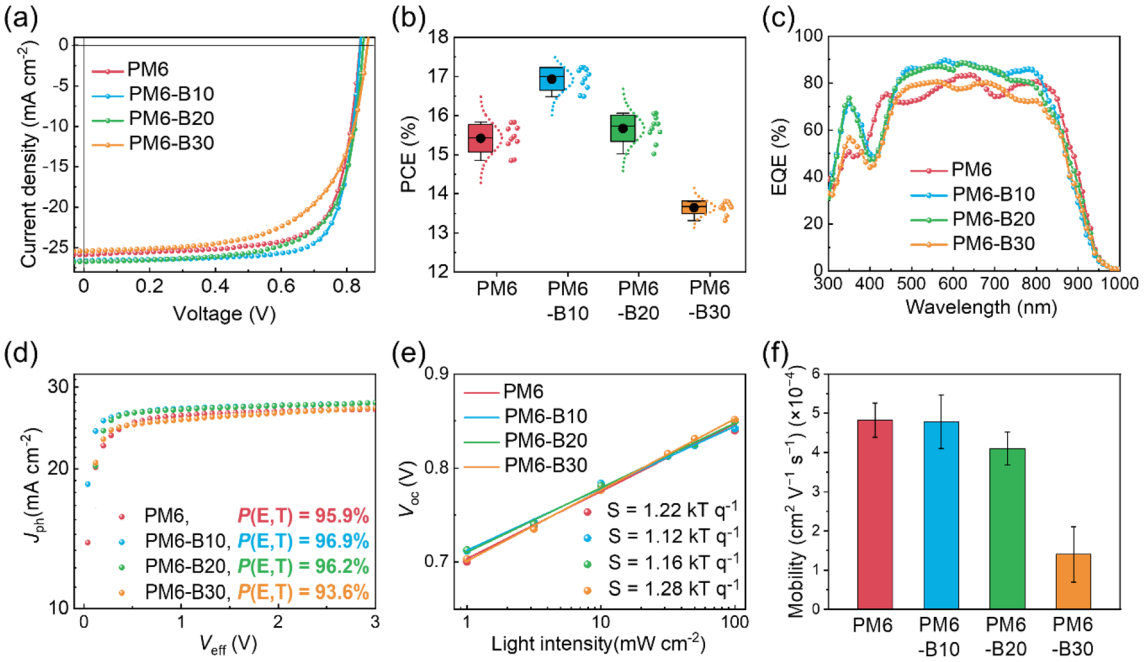

Fig. 2 Photovoltaic performance of P_D:Y6-BO OSCs; (a) *J*–*V* curves, (b) PCE distribution, (c) EQE spectra, (d) J_{ph} *vs.* V_{eff} curves and (e) light intensity-dependent V_{oc}. (f) Hole mobilities of P_D:Y6-BO blend films.

those of the other P_Ds was synthesized (Table S3†). The photovoltaic performance of PM6-P10:Y6-BO OSCs (V_{oc} = 0.85 V, J_{sc} = 25.04 mA cm^{-2}, FF = 0.65, and PCE = 13.77%) was significantly poorer than those of PM6:Y6-BO and PM6-B10:Y6-BO devices (Table S4†), which can be mainly attributed to the inferior μ_h of PM6-P10 (0.8×10^{-4} cm^2 V^{-1} s^{-1}).[8,56] This result confirms the importance of introducing BID unit as the third component of terpolymer donors for achieving high-performance OSCs.

To elucidate the origin of the different photovoltaic performances depending on P_Ds, the charge generation and recombination properties of the OSCs were investigated (Fig. 2d, e and S11†). First, the exciton dissociation probability ($P(E,T)$) of each OSC was determined from its photocurrent density (J_{ph})–effective voltage (V_{eff}) curve, calculated by dividing the J_{ph} under short-circuit conditions by the saturated current density (J_{sat}) at V_{eff} = 3 V.[57] The $P(E,T)$s of all the OSCs were in the range of 94–97%, indicating efficient exciton dissociation and charge generation; the PM6-B10:Y6-BO OSC exhibited the highest $P(E,T)$ of 97%, which contributed to its superior J_{sc} (Fig. 2d). The charge recombination properties of the OSCs were investigated by examining their light intensity (P_{light})–dependent V_{oc} and J_{sc}. In general, the slope (S) of V_{oc}–log P_{light} plot, with unit of k_BT/q (k_B = Boltzmann constant, T = temperature in Kelvin, and q = elementary charge), and the slope (α) of log J_{sc}–log P_{light} plot indicate the degrees of monomolecular/trap-assisted and bimolecular recombination of OSCs, respectively.[58–60] The S and α values associated with the PM6-B10:Y6-BO ($S = 1.12\ k_BT/q$, α = 0.91) and PM6-B20:Y6-BO ($S = 1.16\ k_BT/q$, α = 0.90) OSCs were nearer to unity ($S = 1\ k_BT/q$ and $\alpha = 1$) than those of the PM6:Y6-BO OSC ($S = 1.22\ k_BT/q$, α = 0.88), suggesting that the degrees of monomolecular/trap-assisted and bimolecular recombination of those OSCs are comparatively low (Fig. 2e and S11†). However, the PM6-B30:Y6-BO OSC showed more severe monomolecular/trap-assisted recombination behavior ($S = 1.28\ k_BT/q$) compared to the PM6:Y6-BO OSC, explaining its low J_{sc} and FF.

To compare the charge transport ability of each blend film, its μ_h and electron mobility (μ_e) were measured using the SCLC method (Fig. 2f and Table S5†). The μ_hs of the PM6:Y6-BO, PM6-B10:Y6-BO, PM6-B20:Y6-BO, and PM6-B30:Y6-BO blend films were $(4.8 \pm 0.4) \times 10^{-4}$, $(4.8 \pm 0.7) \times 10^{-4}$, $(4.1 \pm 0.4) \times 10^{-4}$, and $(1.4 \pm 0.7) \times 10^{-4}$ cm^2 V^{-1} s^{-1}, respectively. Interestingly,

Table 2 Photovoltaic performance of P_D:Y6-BO OSCs

P_Ds	V_{oc} [V]	J_{sc} [mA cm^{-2}]	Calc. J_{sc}[a] [mA cm^{-2}]	FF	PCE$_{max}$ (PCE$_{avg}$)[b] [%]
PM6	0.84	25.85	25.75	0.73	15.83 (15.42 ± 0.35)
PM6-B10	0.84	26.60	26.81	0.77	17.23 (16.94 ± 0.28)
PM6-B20	0.85	26.72	26.53	0.71	16.06 (15.67 ± 0.34)
PM6-B30	0.86	25.42	24.34	0.63	13.80 (13.65 ± 0.16)

[a] Calculated from the EQE spectra. [b] Average values based on at least 10 devices.

the μ_h of the PM6-B10:Y6-BO blend film was comparable to that of the PM6:Y6-BO blend film, showing a well-balanced electron–hole mobility (μ_e/μ_h = 1.2). These results indicate that the presence of the electro-active BID units in PM6-B10 does not compromise its electrical properties.[61–63] The balanced electron–hole mobility (μ_e/μ_h) of the PM6-B10:Y6-BO blend film is consistent with the low degree of charge recombination and high FF in OSCs.

2.3. Morphological properties of blend films

To further elucidate the differences in the photovoltaic performances of the OSCs depending on the P_Ds, we investigated the morphological characteristics of the P_D:Y6-BO blend films by GIXS, resonant soft X-ray scattering (RSoXS), differential scanning calorimetry (DSC), and contact angle measurements. First, we found that the P_D:Y6-BO blend films showed similar crystalline properties (Fig. S12 and Table S6†). For example, the PM6 and PM6-BX (X = 10, 20, and 30)-based blend films showed dominantly face-on oriented packing structures, as confirmed by distinct (100) peaks along the IP direction and (010) peaks along the OOP direction in the GIXS linecut profiles. Also, the L_c values of the terpolymer-based blend films were relatively well-maintained ($L_{c(100)}$ = 6.3 nm and $L_{c(010)}$ = 2.4 nm for PM6:Y6-BO and $L_{c(100)}$ = 5.2 nm and $L_{c(010)}$ = 2.3 nm for PM6-B20:Y6-BO) (Table S6†). Interestingly, a significant difference in the morphological characteristics between PM6 and terpolymers was found in the RSoXS results in terms of domain purity and size of the blend films (Fig. 3a and Table 3).[64] The RSoXS profiles were obtained with a beam energy of 285.2 eV to maximize the contrast between the P_D and S_A. The evaluation of the relative domain purity of the blend films is described in the ESI.†[65] The RSoXS profile of the PM6:Y6-BO blend film exhibited a strong scattering peak at q value of 0.010 Å^{-1} (corresponding to domain spacing of 63 nm, domain spacing = $2\pi/q_{peak}$). In contrast, the peaks were much less distinct in the RSoXS profiles of the PM6-B10:Y6-BO and PM6-B20:Y6-BO blend films; their relative domain purities were only 0.25 and 0.29, respectively, relative to the PM6:Y6-BO blend film (domain purity = 1.00). These results indicate that the incorporation of the BID unit into PM6 induced better-intermixed domains in the blend film. These results explain the higher $P(E,T)$ values of the PM6-B10:Y6-BO and PM6-B20:Y6-BO OSCs.

Table 3 Relative domain purities and DSC results of the P_D:Y6-BO blend films

Materials	Relative domain purity[a]	T_m[b] (°C)	ΔH_m[b] (J g^{-1})
PM6:Y6-BO	1	271	13.0
PM6-B10:Y6-BO	0.25	270, 273	7.9
PM6-B20:Y6-BO	0.29	267	1.5
Y6-BO	—	271	25.7

[a] Estimated using integrated scattering intensity of RSoXS profiles. [b] Determined by DSC.

To support the enhanced intermixing of the P_D and S_A domains in PM6-B10:Y6-BO and PM6-B20:Y6-BO blend films, DSC measurements were performed (Fig. 3b and Table 3). The blend samples for the DSC measurements were prepared using the same conditions as those used for the OSC fabrication. In detail, the blend solutions were spun-cast onto glass substrates and the films were collected in DSC pans. We then compared the DSC thermograms of the samples obtained during the first heating cycle. The DSC thermograms of all blend films exhibited distinct peaks at 265–275 °C, which are associated with the melting transition of Y6-BO.[66,67] The melting enthalpy (ΔH_m) of the blend films gradually decreased with increasing BID content of the P_D. For example, the ΔH_ms of PM6:Y6-BO, PM6-B10:Y6-BO, and PM6-B20:Y6-BO blend films were 13.0, 7.9, and 1.5 J g^{-1}, respectively. These results indicate effectively suppressed crystalline features of the PM6-B10:Y6-BO and PM6-B20:Y6-BO blend films compared to those of the PM6:Y6-BO blend films. The DSC data also support the formation of a larger fraction of

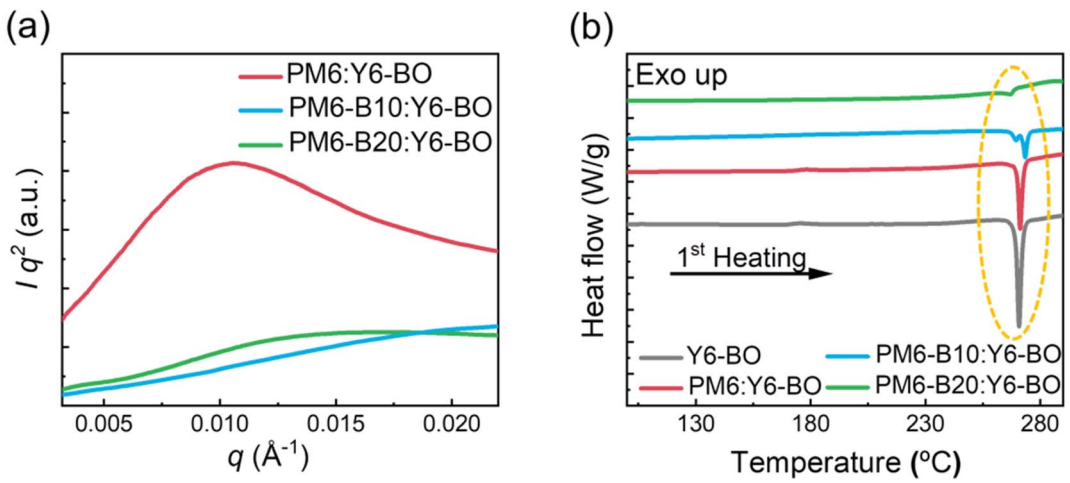

Fig. 3 (a) RSoXS profiles of P_D:Y6-BO blend films. (b) DSC thermograms of Y6-BO and P_D:Y6-BO blend films obtained during the 1st heating cycle.

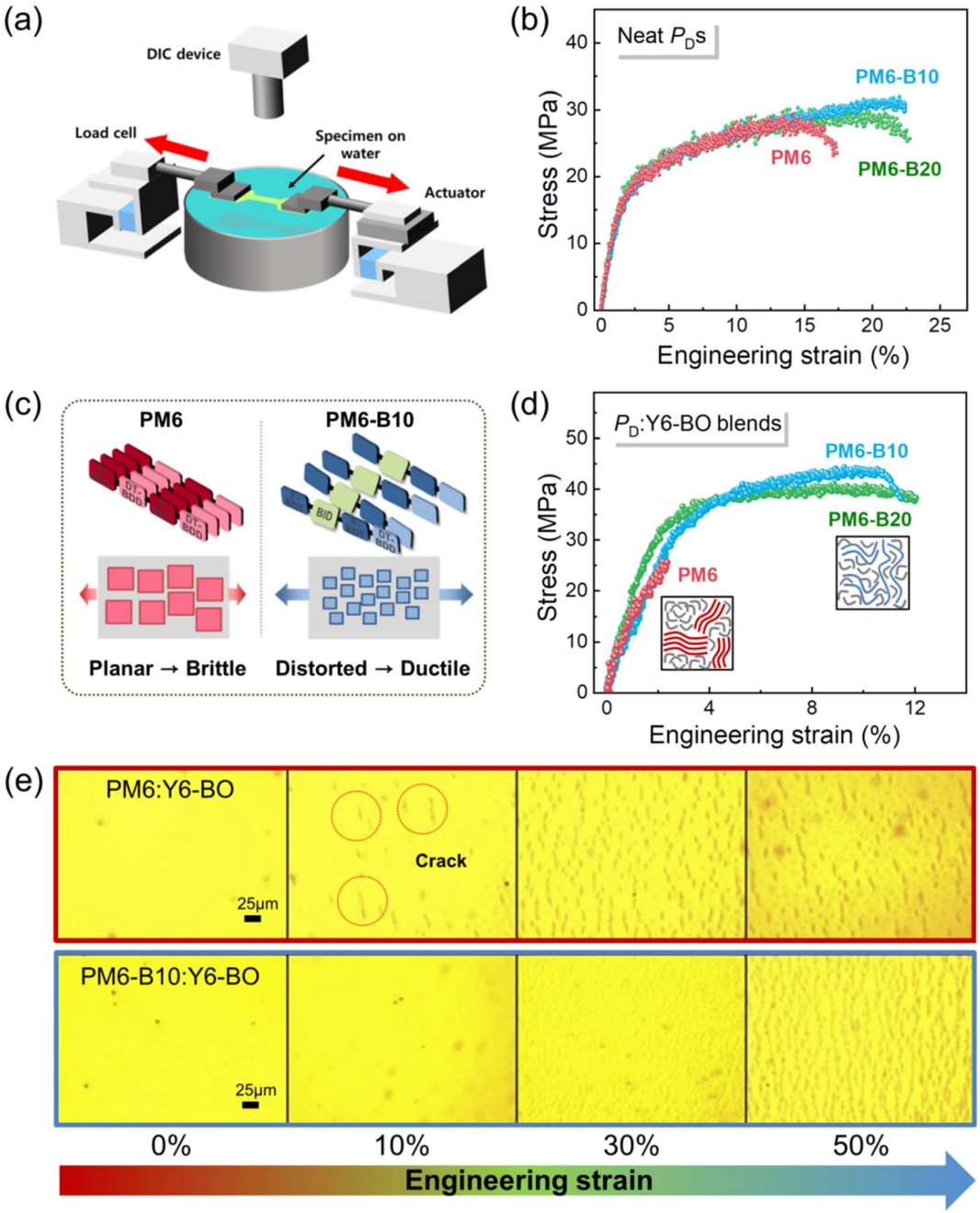

Fig. 4 (a) Schematic of the pseudo free-standing tensile test performed in this study. (b) Stress–strain curves of neat P_D films. (c) Illustration of the impact of BID unit incorporation on the mechanical properties of P_D films. (d) Stress–strain curves of P_D:Y6-BO blend films. (e) Optical microscope (OM) images of P_D:Y6-BO blend films on TPU substrates under stretching.

intermixed P_D/S_A domains in the PM6-B10:Y6-BO and PM6-B20:Y6-BO blend films than in PM6:Y6-BO.[68]

To examine the origin of the well-intermixed P_D and S_A domains in the PM6-B10:Y6-BO and PM6-B20:Y6-BO blend films, we investigated the molecular compatibility of the P_Ds and Y6-BO by estimating their interfacial tension (γ^{D-A}) based on the Wu model (Fig. S13, Tables S7 and S8†).[69–71] The water and glycerol contact angles of the P_Ds and Y6-BO were measured to determine the surface tensions of each material. The γ^{D-A} values of the PM6-B10:Y6-BO and PM6-B20:Y6-BO blend films were 0.46 and 0.43 mN m^{-1}, respectively, which were lower than that of the PM6:Y6-BO blend film (0.93 mN m^{-1}). A low γ^{D-A} value indicates better molecular compatibility between the P_D and S_A at their interface, which facilitates intermixing of the domains. Atomic force microscopy (AFM) measurements were also performed to understand the surface topology of each blend film (Fig. S14†). While similar root-mean-square (RMS) roughness (R_q) values of 2.2–2.6 nm were obtained for the PM6:Y6-BO, PM6-B10:Y6-BO, and PM6-B20:Y6-BO blend films, the PM6-B30:Y6-BO blend film exhibited very rough surface (R_q

= 7.5 nm). This result was mainly due to large aggregates associated with the low solubility of PM6-B30. Accordingly, PM6-B30 was not further considered in the stretchability test below.

2.4. Mechanical properties of neat and blend films

Considering that the molecular packing of P_Ds can have impact on the mechanical properties of their thin films, we investigated the tensile properties (*i.e.*, COS and toughness) of the P_Ds in film using a pseudo free-standing tensile test (Fig. 4a).[72,73] The pseudo free-standing method can minimize interference between the sample and substrate by floating thin films on frictionless water surface, enabling accurate evaluation of the tensile properties. The COS refers to the strain at which cracks first occur, and the toughness indicates the ability to absorb energy up to fracture. As shown in Fig. 4b, the tensile properties of PM6-B10 and PM6-B20 neat films were superior to those of the PM6 film. For example, the COS_{avg} of PM6-B10 (23.8%) and PM6-B20 (22.7%) were significantly higher than that of PM6 (COS_{avg} = 14.9%) (Fig. 4b and Table S9†). Also, the toughness of the neat films increased from 3.5 MJ m^{-3} (PM6) to 5.9 MJ m^{-3} (PM6-B10) and 5.5 MJ m^{-3} (PM6-B20) by 1.6–1.7 times. These results emphasize that the large plastic deformation of BID-incorporated P_D films effectively dissipate a significant amount of strain energy (Fig. 4c). This energy dissipation leads to the prevention of crack generation/propagation in P_D films.

We also investigated the tensile properties of PM6:Y6-BO, PM6-B10:Y6-BO and PM6-B20:Y6-BO blend films (Fig. 4d and Table S9†), which are influenced by both the blend morphologies and tensile properties of the P_D component. As a result, the tensile properties of PM6-B10:Y6-BO and PM6-B20:Y6-BO blend films (COS_{avg} of 11.4 and 12.6%, respectively, and toughness of 4.1 and 4.8 MJ m^{-3}, respectively) were superior to those of PM6:Y6-BO blend film (COS_{avg} = 2.0% and toughness = 0.3 MJ m^{-3}). In particular, the COS_{avg} of the PM6-B10:Y6-BO blend film exceeded that of the PM6:Y6-BO blend film by a factor of five, which is much larger than the difference in the neat P_D films. This result can be attributed to the fact that the mechanical properties of the blend films are determined by both the tensile properties of each constituent and their interfacial properties.[12,20] For example, superior mechanical properties of PM6-B10:Y6-BO and PM6-B20:Y6-BO blend films are attributed to the synergistic effect of better tensile properties of their terpolymer donors and more developed intermixing of their P_D and S_A domains that suppresses crack formation/propagation.

Lastly, to demonstrate the potential of the BID-based P_Ds for stretchable OSC application, the crack formation behavior was monitored while stretching the P_D:Y6-BO blend films mounted on the thermoplastic polyurethane (TPU) substrates (Fig. 4e). It is noteworthy that cracks in the PM6-B10:Y6-BO blend film were barely observed during stretching up to 30% strain, whereas the development of cracks was noticeable in the PM6:Y6-BO blend film at only 10% strain. Thus, this result was consistent with the pseudo free-standing tensile test that the PM6-B10:Y6-BO blend film exhibited superior resistance to crack propagation under mechanical stress. The high stretchability of the PM6-B10:Y6-BO blend film on the substrate demonstrates its high feasibility for the application in stretchable OSCs.

3. Conclusions

In this study, we developed a highly efficient and mechanically robust terpolymer donors featuring an electro-active third component (BID). The incorporation of 10 mol% BID in PM6 produced a PM6-B10 with optimized rigidity and crystallinity, leading to superior electrical and mechanical properties in film ($\mu_h = 3.2 \times 10^{-4}$ cm^2 V^{-1} s^{-1}, COS_{avg} = 23.8%, and toughness = 5.9 MJ m^{-3}). Importantly, these beneficial features of PM6-B10 were reflected in its blend with Y6-BO. The PM6-B10:Y6-BO OSC demonstrated a higher PCE (17.2%) than the PM6:Y6-BO OSC (PCE = 15.8%), with improved charge generation and recombination properties. The mechanical properties of the PM6-B10:Y6-BO blend film (COS_{avg} = 11.4% and toughness = 4.1 MJ m^{-3}) were also superior to those of the PM6:Y6-BO blend film (COS_{avg} = 2.0% and toughness = 0.3 MJ m^{-3}) due to the combined contribution of the high ductility of PM6-B10 and enhanced intermixing of P_D and S_A domains. Therefore, the results of this study demonstrate the effectiveness of incorporating an optimal amount of a bulky electro-active third component into P_D for high-performance and mechanically robust OSCs.

Conflicts of interest

The authors declare no conflict of interest.

Acknowledgements

This research was supported by the National Research Foundation of Korea (2017M3A7B8065584, 2020M3D1A2102869 and 2017M3D1A1039553). This research is additionally performed as a cooperation project of "Basic project", supported by the Korea Research Institute of Chemical Technology (KRICT). The experiment at the Advanced Light Source was supported by a DOE office of Science User Facility under contract no. DE-AC02-05CH11231.

References

1 A. X. Chen, A. T. Kleinschmidt, K. Choudhary and D. J. Lipomi, *Chem. Mater.*, 2020, **32**, 7582–7601.
2 E. Dauzon, X. Sallenave, C. Plesse, F. Goubard, A. Amassian and T. D. Anthopoulos, *Adv. Mater.*, 2021, **33**, 2101469.
3 R. Ma, S.-Y. Chou, Y. Xie and Q. Pei, *Chem. Soc. Rev.*, 2019, **48**, 1741–1786.
4 J. Qin, L. Lan, S. Chen, F. Huang, H. Shi, W. Chen, H. Xia, K. Sun and C. Yang, *Adv. Funct. Mater.*, 2020, **30**, 2002529.
5 J. S. Park, G.-U. Kim, S. Lee, J.-W. Lee, S. Li, J.-Y. Lee and B. J. Kim, *Adv. Mater.*, 2022, **34**, 2201623.
6 A. D. Printz and D. J. Lipomi, *Appl. Phys. Rev.*, 2016, **3**, 021302.

7 Z. Ding, D. Liu, K. Zhao and Y. Han, *Macromolecules*, 2021, **54**, 3907–3926.
8 P. J. W. Sommerville, Y. Li, B. X. Dong, Y. Zhang, J. W. Onorato, W. K. Tatum, A. H. Balzer, N. Stingelin, S. N. Patel, P. F. Nealey and C. K. Luscombe, *Macromolecules*, 2020, **53**, 7511–7518.
9 G. P. Kini, H. S. Park, S. J. Jeon, Y. W. Han and D. K. Moon, *Sol. Energy*, 2020, **207**, 720–728.
10 B. Zheng, L. Huo and Y. Li, *NPG Asia Mater.*, 2020, **12**, 3.
11 K. Zhou, K. Xian, Q. Qi, M. Gao, Z. Peng, J. Liu, Y. Liu, S. Li, Y. Zhang, Y. Geng and L. Ye, *Adv. Funct. Mater.*, 2022, **32**, 2201781.
12 J.-W. Lee, C. Lim, S.-W. Lee, Y. Jeon, S. Lee, T.-S. Kim, J.-Y. Lee and B. J. Kim, *Adv. Energy Mater.*, 2022, 2202224.
13 B. Roth, S. Savagatrup, N. V. de los Santos, O. Hagemann, J. E. Carlé, M. Helgesen, F. Livi, E. Bundgaard, R. R. Søndergaard, F. C. Krebs and D. J. Lipomi, *Chem. Mater.*, 2016, **28**, 2363–2373.
14 H. You, A. L. Jones, B. S. Ma, G.-U. Kim, S. Lee, J.-W. Lee, H. Kang, T.-S. Kim, J. R. Reynolds and B. J. Kim, *J. Mater. Chem. A*, 2021, **9**, 2775–2783.
15 M. U. Ocheje, M. Selivanova, S. Zhang, T. H. Van Nguyen, B. P. Charron, C.-H. Chuang, Y.-H. Cheng, B. Billet, S. Noori, Y.-C. Chiu, X. Gu and S. Rondeau-Gagné, *Polym. Chem.*, 2018, **9**, 5531–5542.
16 Y.-W. Huang, Y.-C. Lin, H.-C. Yen, C.-K. Chen, W.-Y. Lee, W.-C. Chen and C.-C. Chueh, *Chem. Mater.*, 2020, **32**, 7370–7382.
17 F. Zhao, Y. Yuan, Y. Ding, Y. Wang, X. Wang, G. Zhang, X. Gu and L. Qiu, *Macromolecules*, 2021, **54**, 5440–5450.
18 E. L. Melenbrink, K. M. Hilby, K. Choudhary, S. Samal, N. Kazerouni, J. L. McConn, D. J. Lipomi and B. C. Thompson, *ACS Appl. Polym. Mater.*, 2019, **1**, 1107–1117.
19 E. L. Melenbrink, K. M. Hilby, M. A. Alkhadra, S. Samal, D. J. Lipomi and B. C. Thompson, *ACS Appl. Mater.*, 2018, **10**, 32426–32434.
20 J.-W. Lee, D. Jeong, D. J. Kim, T. N.-L. Phan, J. S. Park, T.-S. Kim and B. J. Kim, *Energy Environ. Sci.*, 2021, **14**, 4067–4076.
21 D. Liu, J. Mun, G. Chen, N. J. Schuster, W. Wang, Y. Zheng, S. Nikzad, J.-C. Lai, Y. Wu, D. Zhong, Y. Lin, Y. Lei, Y. Chen, S. Gam, J. W. Chung, Y. Yun, J. B. H. Tok and Z. Bao, *J. Am. Chem. Soc.*, 2021, **143**, 11679–11689.
22 D. Liu, Y. Lei, X. Ji, Y. Wu, Y. Lin, Y. Wang, S. Zhang, Y. Zheng, Y. Chen, J.-C. Lai, D. Zhong, H.-W. Cheng, J. A. Chiong, X. Gu, S. Gam, Y. Yun, J. B. H. Tok and Z. Bao, *Adv. Funct. Mater.*, 2022, 2203527.
23 J.-W. Lee, C. Sun, S.-W. Lee, G.-U. Kim, S. Li, C. Wang, T.-S. Kim, Y.-H. Kim and B. J. Kim, *Energy Environ. Sci.*, 2022, **15**, 4672–4685.
24 J.-W. Lee, C. Sun, B. S. Ma, H. J. Kim, C. Wang, J. M. Ryu, C. Lim, T.-S. Kim, Y.-H. Kim, S.-K. Kwon and B. J. Kim, *Adv. Energy Mater.*, 2021, **11**, 2003367.
25 J.-W. Lee, G.-U. Kim, D. J. Kim, Y. Jeon, S. Li, T.-S. Kim, J.-Y. Lee and B. J. Kim, *Adv. Energy Mater.*, 2022, **12**, 2200887.
26 Z. Peng, K. Jiang, Y. Qin, M. Li, N. Balar, B. T. O'Connor, H. Ade, L. Ye and Y. Geng, *Adv. Energy Mater.*, 2021, **11**, 2003506.
27 R. Ma, K. Zhou, Y. Sun, T. Liu, Y. Kan, Y. Xiao, T. A. Dela Peña, Y. Li, X. Zou, Z. Xing, Z. Luo, K. S. Wong, X. Lu, L. Ye, H. Yan and K. Gao, *Matter*, 2022, **5**, 725–734.
28 J. Wang, C. Han, F. Bi, D. Huang, Y. Wu, Y. Li, S. Wen, L. Han, C. Yang, X. Bao and J. Chu, *Energy Environ. Sci.*, 2021, **14**, 5968–5978.
29 L.-H. Chou, T. Mikie, M. Saito, C.-L. Liu and I. Osaka, *ACS Appl. Mater.*, 2022, **14**, 14400–14409.
30 J. Zhang, Q. Huang, K. Zhang, T. Jia, J. Jing, Y. Chen, Y. Li, Y. Chen, X. Lu, H. Wu, F. Huang and Y. Cao, *Energy Environ. Sci.*, 2022, **15**, 4561–4571.
31 X. Yuan, Y. Zhao, D. Xie, L. Pan, X. Liu, C. Duan, F. Huang and Y. Cao, *Joule*, 2022, **6**, 647–661.
32 M. Zhang, X. Guo, W. Ma, H. Ade and J. Hou, *Adv. Mater.*, 2015, **27**, 4655–4660.
33 Q. Guo, Q. Guo, Y. Geng, A. Tang, M. Zhang, M. Du, X. Sun and E. Zhou, *Mater. Chem. Front.*, 2021, **5**, 3257–3280.
34 R. Yu, G. Wu and Z. Tan, *J. Energy Chem.*, 2021, **61**, 29–46.
35 Y. Cui, H. Yao, L. Hong, T. Zhang, Y. Xu, K. Xian, B. Gao, J. Qin, J. Zhang, Z. Wei and J. Hou, *Adv. Mater.*, 2019, **31**, 1808356.
36 W. Peng, Y. Lin, S. Y. Jeong, Z. Genene, A. Magomedov, H. Y. Woo, C. Chen, W. Wahyudi, Q. Tao, J. Deng, Y. Han, V. Getautis, W. Zhu, T. D. Anthopoulos and E. Wang, *Nano Energy*, 2022, **92**, 106681.
37 Z. Zhang, J. Miao, Z. Ding, B. Kan, B. Lin, X. Wan, W. Ma, Y. Chen, X. Long, C. Dou, J. Zhang, J. Liu and L. Wang, *Nat. Commun.*, 2019, **10**, 3271.
38 J. Y. Oh, S. Rondeau-Gagné, Y.-C. Chiu, A. Chortos, F. Lissel, G.-J. N. Wang, B. C. Schroeder, T. Kurosawa, J. Lopez, T. Katsumata, J. Xu, C. Zhu, X. Gu, W.-G. Bae, Y. Kim, L. Jin, J. W. Chung, J. B. H. Tok and Z. Bao, *Nature*, 2016, **539**, 411–415.
39 S. Savagatrup, X. Zhao, E. Chan, J. Mei and D. J. Lipomi, *Macromol. Rapid Commun.*, 2016, **37**, 1623–1628.
40 Y.-C. Lin, M. Matsuda, C.-K. Chen, W.-C. Yang, C.-C. Chueh, T. Higashihara and W.-C. Chen, *Macromolecules*, 2021, **54**, 7388–7399.
41 Z. Genene, J.-W. Lee, S.-W. Lee, Q. Chen, Z. Tan, B. A. Abdulahi, D. Yu, T.-S. Kim, B. J. Kim and E. Wang, *Adv. Mater.*, 2022, **34**, 2107361.
42 J. Wu, G. Li, J. Fang, X. Guo, L. Zhu, B. Guo, Y. Wang, G. Zhang, L. Arunagiri, F. Liu, H. Yan, M. Zhang and Y. Li, *Nat. Commun.*, 2020, **11**, 4612.
43 S. Seo, J. Kim, H. Kang, J.-W. Lee, S. Lee, G.-U. Kim and B. J. Kim, *Macromolecules*, 2021, **54**, 53–63.
44 H. Hu, P. C. Y. Chow, G. Zhang, T. Ma, J. Liu, G. Yang and H. Yan, *Acc. Chem. Res.*, 2017, **50**, 2519–2528.
45 J. Mun, Y. Ochiai, W. Wang, Y. Zheng, Y.-Q. Zheng, H.-C. Wu, N. Matsuhisa, T. Higashihara, J. B. H. Tok, Y. Yun and Z. Bao, *Nat. Commun.*, 2021, **12**, 3572.
46 C. J. Brabec, A. Cravino, D. Meissner, N. S. Sariciftci, T. Fromherz, M. T. Rispens, L. Sanchez and J. C. Hummelen, *Adv. Funct. Mater.*, 2001, **11**, 374–380.

47 Y. Li, M. Kim, Z. Wu, C. Lee, Y. W. Lee, J.-W. Lee, Y. J. Lee, E. Wang, B. J. Kim and H. Y. Woo, *J. Mater. Chem. C*, 2019, **7**, 1681–1689.
48 J. R. Tumbleston, B. A. Collins, L. Yang, A. C. Stuart, E. Gann, W. Ma, W. You and H. Ade, *Nat. Photonics*, 2014, **8**, 385–391.
49 J. Rivnay, S. C. B. Mannsfeld, C. E. Miller, A. Salleo and M. F. Toney, *Chem. Rev.*, 2012, **112**, 5488–5519.
50 Z. Chiguvare and V. Dyakonov, *Phys. Rev. B: Condens. Matter Mater. Phys.*, 2004, **70**, 235207.
51 J. Yao, B. Qiu, Z.-G. Zhang, L. Xue, R. Wang, C. Zhang, S. Chen, Q. Zhou, C. Sun, C. Yang, M. Xiao, L. Meng and Y. Li, *Nat. Commun.*, 2020, **11**, 2726.
52 L. Hong, H. Yao, Z. Wu, Y. Cui, T. Zhang, Y. Xu, R. Yu, Q. Liao, B. Gao, K. Xian, H. Y. Woo, Z. Ge and J. Hou, *Adv. Mater.*, 2019, **31**, 1903441.
53 Y. Li, W. K. Tatum, J. W. Onorato, Y. Zhang and C. K. Luscombe, *Macromolecules*, 2018, **51**, 6352–6358.
54 Y. Li, W. K. Tatum, J. W. Onorato, S. D. Barajas, Y. Y. Yang and C. K. Luscombe, *Polym. Chem.*, 2017, **8**, 5185–5193.
55 K.-J. Baeg, J. Kim, D. Khim, M. Caironi, D.-Y. Kim, I.-K. You, J. R. Quinn, A. Facchetti and Y.-Y. Noh, *ACS Appl. Mater.*, 2011, **3**, 3205–3214.
56 J. S. Park, G.-U. Kim, D. Lee, S. Lee, B. Ma, S. Cho and B. J. Kim, *Adv. Funct. Mater.*, 2020, **30**, 2005787.
57 V. Shrotriya, Y. Yao, G. Li and Y. Yang, *Appl. Phys. Lett.*, 2006, **89**, 063505.
58 L. J. A. Koster, M. Kemerink, M. M. Wienk, K. Maturová and R. A. J. Janssen, *Adv. Mater.*, 2011, **23**, 1670–1674.
59 H. Jiang, C. Han, Y. Li, F. Bi, N. Zheng, J. Han, W. Shen, S. Wen, C. Yang, R. Yang and X. Bao, *Adv. Funct. Mater.*, 2021, **31**, 2007088.
60 G. A. H. Wetzelaer, M. Kuik, M. Lenes and P. W. M. Blom, *Appl. Phys. Lett.*, 2011, **99**, 153506.
61 Y. Zheng, G.-J. N. Wang, J. Kang, M. Nikolka, H.-C. Wu, H. Tran, S. Zhang, H. Yan, H. Chen, P. Y. Yuen, J. Mun, R. H. Dauskardt, I. McCulloch, J. B. H. Tok, X. Gu and Z. Bao, *Adv. Funct. Mater.*, 2019, **29**, 1905340.
62 R. Noriega, J. Rivnay, K. Vandewal, F. P. V. Koch, N. Stingelin, P. Smith, M. F. Toney and A. Salleo, *Nat. Mater.*, 2013, **12**, 1038–1044.
63 S. Himmelberger and A. Salleo, *MRS Commun.*, 2015, **5**, 383–395.
64 S. Mukherjee, C. M. Proctor, J. R. Tumbleston, G. C. Bazan, T.-Q. Nguyen and H. Ade, *Adv. Mater.*, 2015, **27**, 1105–1111.
65 C. Lee, T. Giridhar, J. Choi, S. Kim, Y. Kim, T. Kim, W. Lee, H.-H. Cho, C. Wang, H. Ade and B. J. Kim, *Chem. Mater.*, 2017, **29**, 9407–9415.
66 Z. Abbas, S. U. Ryu, M. Haris, C. E. Song, H. K. Lee, S. K. Lee, W. S. Shin, T. Park and J.-C. Lee, *Nano Energy*, 2022, **101**, 107574.
67 M. Zhang, L. Zhu, T. Hao, G. Zhou, C. Qiu, Z. Zhao, N. Hartmann, B. Xiao, Y. Zou, W. Feng, H. Zhu, M. Zhang, Y. Zhang, Y. Li, T. P. Russell and F. Liu, *Adv. Mater.*, 2021, **33**, 2007177.
68 L. Ye, H. Hu, M. Ghasemi, T. Wang, B. A. Collins, J.-H. Kim, K. Jiang, J. H. Carpenter, H. Li, Z. Li, T. McAfee, J. Zhao, X. Chen, J. L. Y. Lai, T. Ma, J.-L. Bredas, H. Yan and H. Ade, *Nat. Mater.*, 2018, **17**, 253–260.
69 J. Comyn, *Int. J. Adhes. Adhes.*, 1992, **12**, 145–149.
70 S. Wu, *J. Polym. Sci., Part C: Polym. Symp.*, 1971, **34**, 19–30.
71 C. Han, J. Wang, S. Zhang, L. Chen, F. Bi, J. Wang, C. Yang, P. Wang, Y. Li and X. Bao, *Adv. Mater.*, 2023, 2208986.
72 J.-H. Kim, A. Nizami, Y. Hwangbo, B. Jang, H.-J. Lee, C.-S. Woo, S. Hyun and T.-S. Kim, *Nat. Commun.*, 2013, **4**, 2520.
73 W. Kim, J. Choi, J.-H. Kim, T. Kim, C. Lee, S. Lee, M. Kim, B. J. Kim and T.-S. Kim, *Chem. Mater.*, 2018, **30**, 2102–2111.